

# Characteristics of miniature pulsed penning ion source: Experiment and PIC simulation

Cite as: Rev. Sci. Instrum. **90**, 123310 (2019); <https://doi.org/10.1063/1.5127921>

Submitted: 25 September 2019 . Accepted: 02 December 2019 . Published Online: 20 December 2019

N. V. Mamedov , A. S. Rohmanenkov, V. I. Zverev , S. P. Maslennikov , A. A. Solodovnikov, A. A. Uzvolok, and D. I. Yurkov



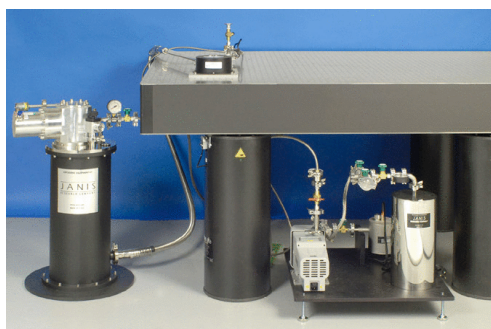
View Online



Export Citation



CrossMark



## JANIS

**Rising LHe costs? Janis has a solution.**  
Janis' Recirculating Cryocooler eliminates the use of Liquid Helium for "wet" cryogenic systems.

[sales@janis.com](mailto:sales@janis.com) [www.janis.com](http://www.janis.com) [Click for more information.](#)

# Characteristics of miniature pulsed penning ion source: Experiment and PIC simulation

Cite as: Rev. Sci. Instrum. 90, 123310 (2019); doi: 10.1063/1.5127921

Submitted: 25 September 2019 • Accepted: 2 December 2019 •

Published Online: 20 December 2019



N. V. Mamedov,<sup>1,2,a)</sup>  A. S. Rohmanenkov,<sup>1</sup> V. I. Zverev,<sup>1,2</sup>  S. P. Maslennikov,<sup>1,2</sup>  A. A. Solodovnikov,<sup>1</sup>  
A. A. Uzvolok,<sup>1</sup> and D. I. Yurkov<sup>1,2</sup>

## AFFILIATIONS

<sup>1</sup>All-Russia Research Institute of Automatics (VNIIA), Sushchevskaya st. 22, Moscow 127055, Russia

<sup>2</sup>National Research Nuclear University MEPhI, Kashirskoe st., 31, Moscow 115409, Russia

**Note:** Contributed paper, published as part of the Proceedings of the 18th International Conference on Ion Sources, Lanzhou, China, September 2019.

<sup>a)</sup>Author to whom correspondence should be addressed: [m\\_nikitos@mail.ru](mailto:m_nikitos@mail.ru)

## ABSTRACT

In the present work, the results of the experimental and particle in cell (PIC) simulation studies of the discharge combustion modes in a miniature Penning ion source (PIS) under the pulse-periodic power supply conditions are presented. Dynamics of discharge ignition and discharge operation mode at a pulsed anode voltage supply are investigated for different values of anode voltage and gas pressure in various magnetic field configurations. Typical examples of current pulse waveforms are shown. Also, numerical simulations of the PIS were performed using 3D PIC combined with Monte Carlo collisions in the code VSim. Temporal dependencies of electron, ion, and potential distributions in the Penning cell are simulated. Differences between the numerical and experimental results are discussed.

Published under license by AIP Publishing. <https://doi.org/10.1063/1.5127921>

## INTRODUCTION

The Penning ion source (PIS) is used in various fields of science and technology due to its simplicity and reliability. PIS was first used in the miniature linear accelerator in 1937 by Penning and Moubis to obtain the D-D nuclear reaction and generate neutrons.<sup>1</sup> Nowadays, due to the simple design and power supply system, as well as reliable operation at low working-gas pressures, the PIS is widely used in the neutron generation systems (in the sealed-tube neutron generators).<sup>2</sup>

The modes of Penning discharge with the cylindrical anode and constant anode voltage have thoroughly been described in Refs. 3 and 4. However, there is not enough information about the extracted ion current behavior; also, all results are obtained for the stationary modes of anode power supply. In this paper, dynamics of discharge ignition and discharge operation mode are investigated at the pulsed anode voltage supply. The influence of the anode voltage amplitude, pulse frequency, pulse duration, and magnetic field configuration on the amplitude-time and current-voltage characteristics of the PIS is studied. The discharge operation modes of PIS and the corresponding ranges of gas pressures, at which various Penning discharge modes are realized, are revealed.

## EXPERIMENTAL AND PIC SIMULATION SETUP

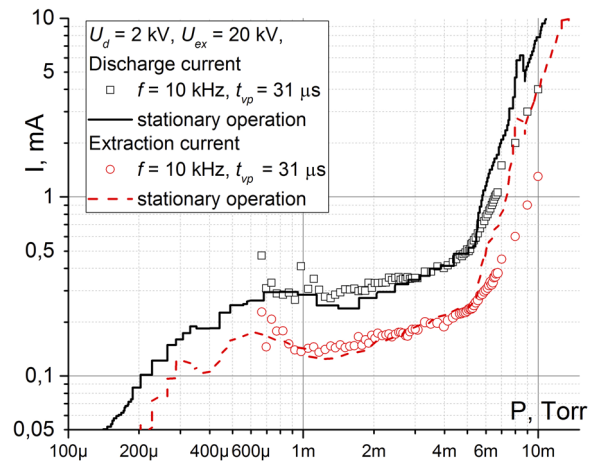
The description of the high vacuum setup for the Penning ion source main parameter measurements used in the present study can be found in Ref. 5. The size of the investigated ion source described in detail in previous papers<sup>6,7</sup> is about  $15 \times \varnothing 12$  mm. A current solenoid or permanent magnets were used to generate an axially symmetric magnetic field (of various induction and configuration) in the PIS. The optimal magnetic field configuration is slightly inhomogeneous with a magnetic field induction of 80–90 mT. The amplitude and time parameter measurements of the discharge current ( $I_d$ ) and the extracted ion current ( $I_{ex}$ ) were performed in the gas pressure range  $P = 0.1$ – $10$  mTorr (working gas is  $H_2$ ). The anode voltage pulse frequency ( $f$ ) and the voltage amplitude ( $U_a$ ) were varied from 0.2 to 10 kHz and 1.5–3.0 kV correspondingly, the pulse duration adjustment range was  $t_{vp} = 30$ – $200$   $\mu$ s, and the accelerating voltage was fixed at  $U_{ex} = -20$  kV.

The 3D electrostatic Particle-In-Cell (PIC) code utilizing structured rectangular grids implemented in the VSim<sup>8</sup> software package was used to simulate Penning gas discharge in the given experimental geometry. In this code,<sup>9</sup> the Monte Carlo collision (MCC) method was used to simulate the kinetic processes in a gas-discharge

plasma. The cell sizes for 3D calculations were 0.50 mm, 0.33 mm, and 0.25 mm. For all the numerical simulations, the time step was 10 ps. The following elementary processes were accounted for: the elastic electron scattering on  $H_2$  molecules, electron impact ionization of  $H_2$  molecules,  $H_2^+$  charge exchange with  $H_2$  molecules,  $H_2^+$  momentum exchange with  $H_2$  molecules, and impact ionization of  $H_2$  molecules by  $H_2^+$ . At the beginning of the numerical simulation,  $\sim 100\,000$  macroelectrons and  $\sim 100\,000$   $H_2^+$  ions were placed in the anode cylindrical region. The initial value of charged particle density is  $2 \times 10^{14} \text{ m}^{-3}$ . The initial velocities of the macroparticles were sampled using the Maxwell distribution at 300 K. The real geometry of the PIS and the experimentally measured magnetic field were used in simulations.

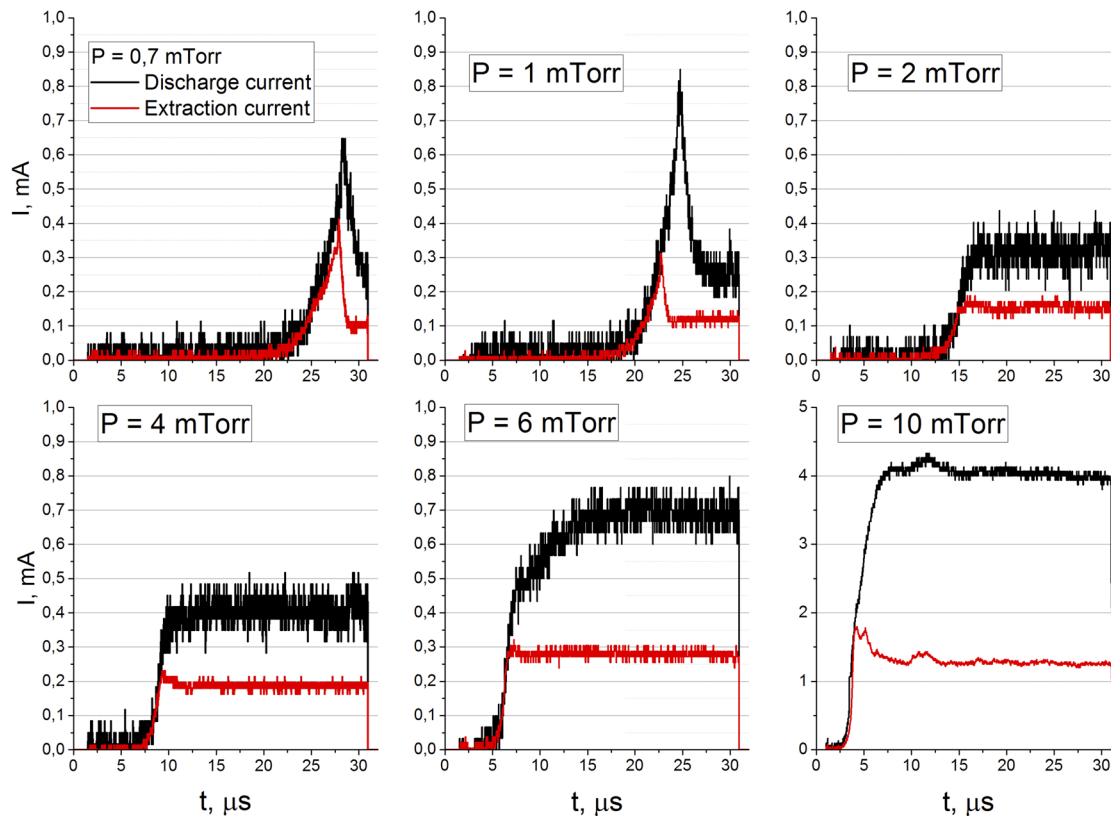
## EXPERIMENTAL AND PIC SIMULATION RESULTS

Figure 1 shows typical examples of the current pulse waveforms obtained for different pressures. In Fig. 2, the  $I_{ex}$  and  $I_d$  amplitudes are plotted as functions of pressure in the discharge cell. Figure 2 was plotted based on measured current pulses. As can be seen, the anode current released on the plateau (in the pulsed mode of supply) is equivalent to the current in the continuous mode of supply at the same gas pressure. In the low pressure range ( $p \leq 1$  mTorr), short-term triangular bursts are observed in the current pulse peak. The current delay time [ $t_{delay}$  is defined as the time between the rising



**FIG. 2.** Discharge current  $I_d$ , and extracted current  $I_{ex}$ , as a function of pressure ( $U_a = 2.0$  kV,  $f = 10$  kHz,  $t_{vp} = 31 \mu\text{s}$ ). Solid lines—DC power supply mode. Points—pulse power supply mode.

edge of anode voltage and the rising edge of current pulse (10% of the plateau)] is more than 20 mks. The triangular burst has longer rise time ( $t_{front}$  is defined as the time between 10% and 90% of the



**FIG. 1.** Typical examples of the current pulse waveforms obtained for different pressures.  $U_a = 2.0$  kV,  $f = 10$  kHz, and  $t_{vp} = 31 \mu\text{s}$ . Point  $t = 0$  is the beginning of the anode voltage pulse.

current pulse height), and it is more than 5 mks. If the pulse duration value is  $t_{vp} = 150\text{--}200\text{ }\mu\text{s}$  and the anode voltage pulse frequency is  $f = 2\text{ kHz}$ , there are typical triangular bursts in the discharge with a frequency of about hundreds of kilohertz to several megahertz in the pressure range of  $p \sim 0.4\text{--}1\text{ mTorr}$ . At higher pressures ( $1\text{ mTorr} < p \leq 6\text{ mTorr}$ ), the discharge current burst becomes trapezoidal, while the extracted current waveform remains rectangular. Characteristic delay times ( $t_{delay}$ ) of the current pulse decreases from 12 to  $5\text{ }\mu\text{s}$ , whereas the current rise time ( $t_{front}$ ) decreases from 2 to  $1.3\text{ }\mu\text{s}$  (see Fig. 3) for pressure increases in the range of 2–8 mTorr.

A further pressure rise ( $p \sim 7\text{ mTorr}$ —exact pressure range depends on the magnetic field) causes an exponential increase in the discharge and extraction current (above 1 mA). In all pressure ranges, the falling edge time does not exceed  $1.3\text{ }\mu\text{s}$ . The accuracy of time measurements is  $\sim 0.3\text{ }\mu\text{s}$ . Following the initial studies of the current-voltage characteristics and the energy and mass spectra of this source,<sup>5,6</sup> it can be assumed that the reason for the discharge (and extraction) current decrease at low pressure and the significant increase at high pressure is transitions between the adjacent discharge modes. The discharge switches from the “low magnetic field” mode to the “transition” mode with possible discharge current fall.<sup>3,4</sup> A further pressure rise leads to transition to the “high-pressure” mode with an exponential increase in the discharge current.<sup>3,4</sup>

The experiments showed a significant effect of the magnetic field strength and structure on the pressure range required for

stable discharge ignition, as well as the amplitude and time characteristics of the discharge and extracted currents. Homogeneous magnetic field ( $B_z \approx 90\text{ mT}$ ) increased the amplitude of the discharge current, but there was no significant decrease in  $t_{delay}$ . The homogeneous magnetic field of higher strength ( $B_z > 100\text{ mT}$ ) led to the change in the combustion discharge mode. The discharge current pulse reached values above 8 mA; at the same time, the extraction current was about 0.3 mA. There was also a time delay ( $5\text{--}10\text{ }\mu\text{s}$ ) between the discharge current pulse start and the extraction current pulse start. The inhomogeneous magnetic field with a linearly decreasing magnetic induction (from cathode to anticathode) improved the current pulse time characteristics, decreased the discharge current, and increased the extraction coefficient.

Figure 3 shows typical examples of the current pulse waveforms obtained via PIC simulations with different gas pressures. One can see from Figs. 1 and 3 that the general form of the simulated current pulses is similar to experimental pulses, but quantitatively values of  $I_{ex}$  and  $I_d$  current amplitudes and time characteristic do not match for the similar pressure level. Simulation current amplitudes are much higher, and current delay time and rise time are much shorter in comparison with the experimental ones. These deviations can be explained by the coarse mesh, small total number of particles, and big initial number of particles. The grid parameters and particle weight were chosen on the verge of stability of the PIC method;<sup>9</sup>

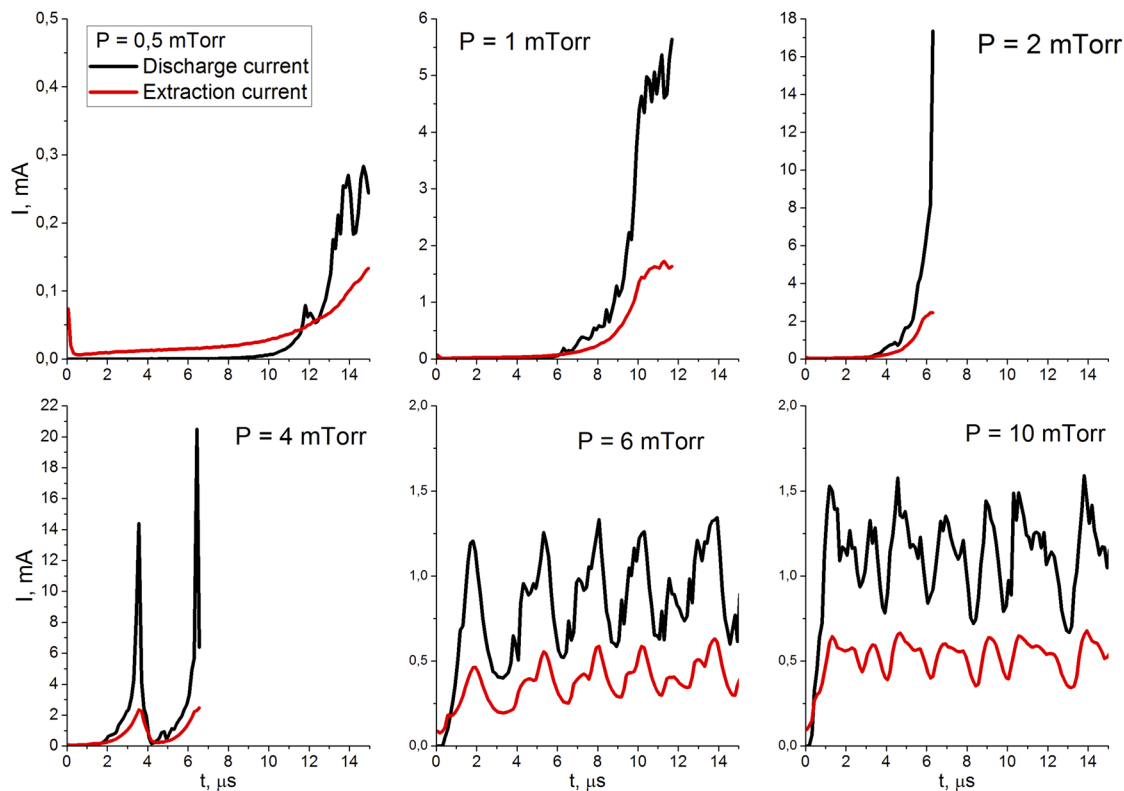


FIG. 3. Typical examples of the simulation current pulse waveforms obtained for different pressures.

therefore, the issues mentioned above cannot be resolved presently. Nevertheless, the simulation of electron, ion, and potential distribution in Penning cell helps to explain qualitatively the fluctuation and triangular burst in current pulses. In Fig. 4, the temporal evolution of the electron distribution is shown for  $p = 4$  and 6 mTorr.

At low pressures (0.5, 1, 2, and 4 mTorr), the current oscillations during the simulation indicate the plasma instability in the Penning discharge (see Fig. 4). Such a current behavior (similar current peaks) is observed in the experimental data with longer pulse time.<sup>5</sup> However, the height of the current peaks in the simulations is overestimated which can be attributed to the large size of the modeling grid cells and the small number of particles in the simulations.

In the simulations, current oscillations for high pressures (6 mTorr and 10 mTorr) are associated with the small number of particles in the modeling. This is the reason behind the current

fluctuating around the average value (see Fig. 3). Unfortunately, increasing the number of particles in the simulations leads to a significant increase in the simulation time and could threaten the stability of the PIC method. Figure 4 (for 6 mTorr) shows quasistationary operation mode in simulations (for high pressure). In quasistationary operation mode simulation, electron density is about  $n_e \sim 2 \times 10^{16} \text{ m}^{-3}$  and the electron temperature is about  $T_e \sim 10\text{--}20 \text{ eV}$ . On the contrary, the experimentally measured (on the basis of the experimentally measured cell center potential<sup>6,10</sup>) electron density is in the range of  $2 \times 10^{15} \text{ m}^{-3}$  to  $8 \times 10^{15} \text{ m}^{-3}$ . For an anode voltage of 2–2.2 kV, the average  $n_e$  is in the range of  $4 \times 10^{15} \text{ m}^{-3}$  to  $7 \times 10^{15} \text{ m}^{-3}$ .<sup>10</sup> Also typical electron temperature for this type of ion source is about  $T_e \sim 5\text{--}10 \text{ eV}$ .<sup>11</sup>

As shown in Fig. 4 (for 6 mTorr), spokes are observed in the electron distribution. These spokes continuously rotate in time. At the same time, ion distribution becomes either

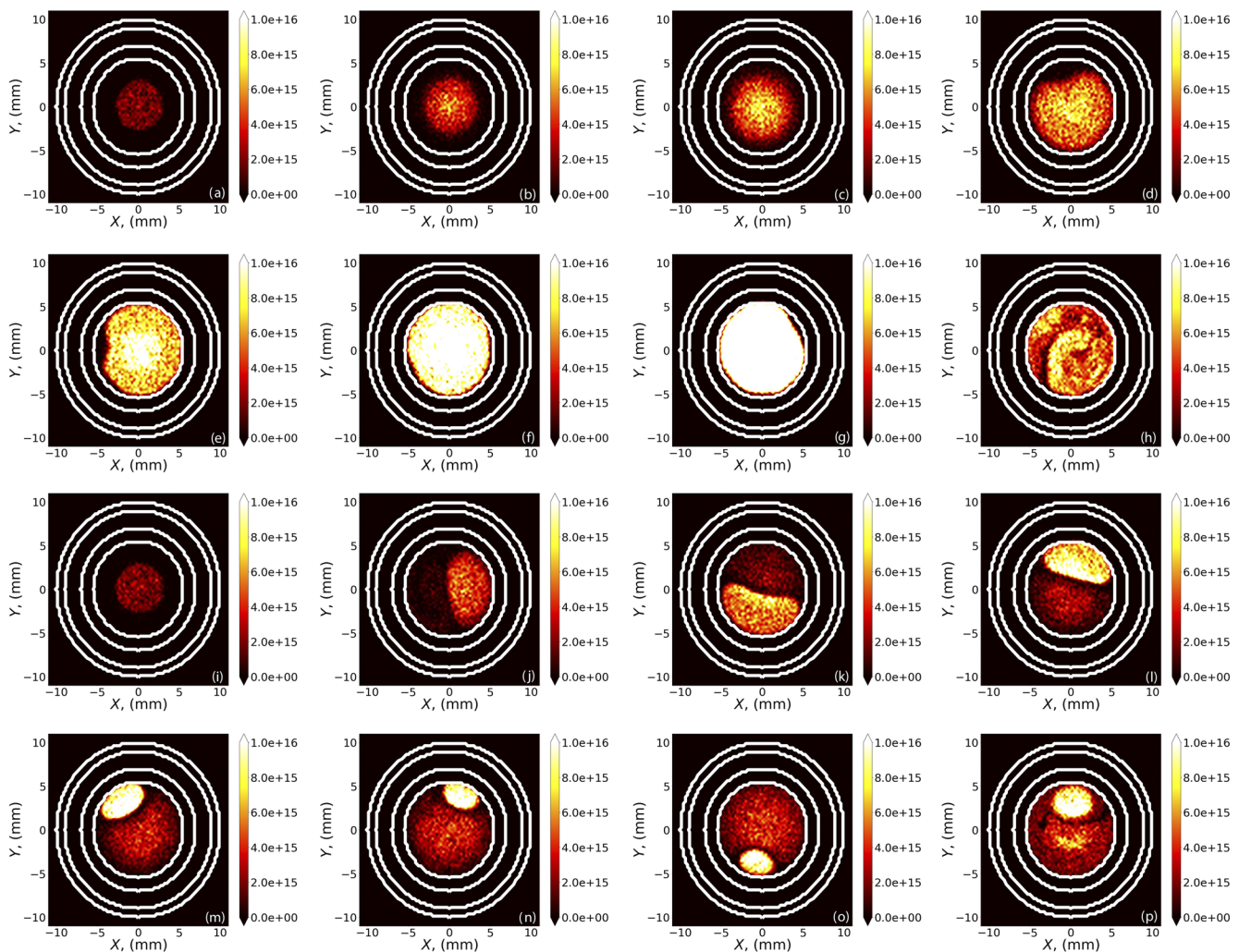


**FIG. 4.** [(a)–(p)] Electron  $n_e$  distributions depending on time. For 4 mTorr, (a)  $t = 0 \mu\text{s}$ , (b)  $t = 0.5 \mu\text{s}$ , (c)  $t = 1.0 \mu\text{s}$ , (d)  $t = 1.5 \mu\text{s}$ , (e)  $t = 2.0 \mu\text{s}$ , (f)  $t = 2.5 \mu\text{s}$ , (g)  $t = 3.0 \mu\text{s}$ , and (h)  $t = 4.0 \mu\text{s}$ . For 6 mTorr, (i)  $t = 0 \mu\text{s}$ , (j)  $t = 0.5 \mu\text{s}$ , (k)  $t = 1.0 \mu\text{s}$ , (l)  $t = 1.5 \mu\text{s}$ , (m)  $t = 2.0 \mu\text{s}$ , (n)  $t = 2.5 \mu\text{s}$ , (o)  $t = 3.0 \mu\text{s}$ , and (p)  $t = 4.0 \mu\text{s}$ .



circular or ring-shaped. The simulation results indicate that the discharge current fluctuation (observed experimentally) results from the disturbance of the axial symmetry of the electric field due to the electron spoke fluctuation during rotation (see Fig. 4 for 4 mTorr). The experimental and theoretical study of the features of these fluctuations is the aim of our future research.

## CONCLUSION

In the present work, the study of the discharge characteristics of the Penning ion source was conducted. The obtained experimental results show the following:

- (a) the anode current released on the plateau (in the pulsed mode of supply) is equivalent to the current in the continuous mode of supply at the same gas pressure,
- (b) the pressure range of the discharge ignition lays within 0.8–1 mTorr; however, at pressures below 2 mTorr, the instability can develop, resulting in the triangular release of the current pulse shape,
- (c) the operating pressures is in the range of 4–6 mTorr. In this range, the discharge is stable, current pulses have regular rectangular shape, and the discharge current increases linearly from about 200 to 500  $\mu\text{A}$  with increasing pressure, whereas the extracted current increases linearly from about 180 to 230 mA. The characteristic delay time of the current pulse ( $t_{\text{delay}}$ ) is in the range of 5–10  $\mu\text{s}$ , and the current rise time ( $t_{\text{front}}$ ) is within 1.3–2  $\mu\text{s}$ . In all pressure ranges, the falling

edge time does not exceed 1.3  $\mu\text{s}$ . The accuracy of time measurements is  $\sim 0.3 \mu\text{s}$ , and

- (d) the increase in the pressure above  $\sim 7$  mTorr (exact pressure range depends on the magnetic field) leads to a sharp exponential increase in the discharge current to values above 1 mA.

Numerical simulations of Penning discharge by the PIC code show that fluctuation of the discharge current arises as a result of the disturbance of the axial symmetry of the potential distribution due to the electron spoke fluctuation.

## REFERENCES

- <sup>1</sup>F. M. Penning and J. H. A. Moubis, "Eine neutronenrohre ohne pumpvorpichtung," *Physica* **4**(11), 71–76 (1937).
- <sup>2</sup>V. Valkovic, *14 MeV Neutrons. Physics and Applications* (CRC Press, Taylor & Francis Group, Boca Raton, London, New York, 2016), p. 500.
- <sup>3</sup>W. Schuurman, *Physica* **36**, 136–1603 (1967).
- <sup>4</sup>E. B. Hooper, "A review of reflex and penning discharges," in *Advances in Electronics and Electron Physics* (Academic Press, New York, 1969), Vol. 27, pp. 295–343.
- <sup>5</sup>N. V. Mamedov *et al.*, *Tech. Phys.* **64**(9), 1290–1297 (2019).
- <sup>6</sup>N. V. Mamedov *et al.*, *Tech. Phys.* **63**(8), 1129–1136 (2018).
- <sup>7</sup>R. S. Rachkov, A. Yu. Presnyakov, and D. I. Yurkov, *At. Energy* **126**(6), 383–387 (2019) [*At. Energ.* 126(6) (2019) (in Russian)].
- <sup>8</sup>C. Nieter and J. R. Cary, *J. Comput. Phys.* **196**, 448 (2004).
- <sup>9</sup>A. S. Rokhmanenkov and S. E. Kuratov, *J. Phys.: Conf. Ser.* **1250**, 012036 (2019).
- <sup>10</sup>N. V. Mamedov *et al.*, *J. Phys.: Conf. Ser.* **755**, 011001 (2016).
- <sup>11</sup>D. Jin *et al.*, *Plasma Sci. Technol.* **11**(1), 48–51 (2009).